Characterization of CuO Supported on Tetragonal ZrO_2 Catalysts for N_2O Decomposition to N_2

Zheng Liu,[†,‡] Michael D. Amiridis,*[,†,§] and Yi Chen*[,‡,⊥]

Department of Chemical Engineering, University of South Carolina, Columbia, South Carolina 29208, and Department of Chemistry, Nanjing University, Nanjing 210093, China

Received: August 11, 2004; In Final Form: November 3, 2004

A series of tetragonal zirconia-supported CuO oxide catalysts with various CuO loadings were characterized by X-ray diffraction (XRD), X-ray photoelectron spectroscopy (XPS), electron spin resonance (ESR), ultraviolet and visible diffuse reflectance spectroscopy (UV/vis−DRS), and temperature-programmed reduction (TPR) measurements. The results indicate that the dispersion capacity of copper oxide on this support is approximately 8.6 Cu^{2+} ions/nm^2 ZrO_2. The state of the resulting supported copper species depends on the CuO loading. At CuO loadings below the dispersion capacity, only highly dispersed copper ion species are present on the surface of t-ZrO_2. In particular, isolated Cu ions are the predominant species at low loadings. In contrast, pair Cu ions become the most abundant species at loadings near the dispersion capacity. It has been proposed that these dispersed CuO (isolated and paired Cu ions) have a symmetric 5-fold-oxygen-coordination symmetry (C_{3v} symmetry) and can be described as distorted octahedra with a missing corner or a trigonal bipyramids. Finally, at CuO loadings above the dispersion capacity the formation of crystalline CuO is observed. TPR results reveal that the dispersed Cu ion species have a different reducibility from CuO crystallites, presumably due to strong interactions between these species and the t-ZrO_2 support. The catalytic activity of these CuO/t-ZrO_2 catalysts for the decomposition of N_2O can also be directly correlated to CuO dispersion, with paired Cu ions being the most active species for this reaction.

Introduction

The properties of supported metal oxides are often different from those of the corresponding bulk metal oxides due to interactions with the supports. The nature of such interactions has been extensively reviewed in the literature.[1−5] Understanding the local structure of the supported active metal oxide phase and the factors that determine this structure has played an important role in developing and optimizing supported metal oxide systems for heterogeneous catalytic applications. Nevertheless, the characterization of the surface structure of supported metal oxides is frequently a complicated task, since several different structures as well as chemical states may coexist in a supported metal oxide system.[6−10]

Supported copper oxide catalysts are extensively used in a variety of chemical processes.[11−18] In recent years, in addition to the alumina and silica supports, efforts have been devoted to the development of titania, ceria, ziconia, and niobia supported CuO catalysts in attempts to adjust the strength of the interaction between the dispersed species and the support.[19−23] In particular, zirconia supported copper oxide exhibits superior performance for the synthesis of methanol from either CO/H_2 or CO_2/H_2 mixtures.[24−26] Nevertheless, relatively little is known regarding the surface and reactivity properties[27−29] of these CuO/ZrO_2 systems.

The catalytic decomposition of nitrous oxide has attracted increasing attention in recent years because of the contribution of nitrous oxide to the destruction of ozone in the stratosphere and its suspected role in the greenhouse effect.[30,31] CuO/ZrO_2 catalysts have exhibited an activity for this reaction, which is comparable to that of the most active catalyst known (Cu−ZSM-5), and a high stability at high N_2O concentrations.[32,33]

The objective of this work is to investigate the structure and reactivity of supported CuO species on tetragonal zirconia. Hence, we have determined the dispersion capacity of CuO on this support by use of XRD and XPS and investigated the structure of the surface species formed. Furthermore, we have explored the chemical properties of the surface dispersed Cu species formed through measurements of their redox properties, as well as their reactivity for the catalytic decomposition of N_2O.

Experimental Section

Tetragonal zirconia (t-ZrO_2) was prepared by a method reported elsewhere.[9,34,35] After calcination at 773 K for 4 h, this material has a BET surface area of 65 m^2/g. Catalysts with different CuO contents were prepared by incipient wetness impregnation using aqueous solutions of cupric nitrate [$Cu(NO_3)_2 \cdot 3H_2O$, A.R.] as precursors. Following impregnation, the catalysts were dried overnight at 373 K and calcined in flowing air at 723 K for 2 h.

X-ray diffraction (XRD) patterns were collected with a Shimadzu XD-3A diffractometer with a Ni-filtered Cu Kα radiation (1.5418 nm). The X-ray tube was operated at 35 kV and 20 mA. Quantitative results were obtained using α-alumina powder as an inner standard.

X-ray photoelectron spectroscopy (XPS) spectra were recorded with a V. G. Escalab MK II system equipped with a hemispherical electron energy analyzer. The spectrometer was operated at 15 kV and 20 mA, and a magnesium anode (Mg

* To whom correspondence should be addressed.
† University of South Carolina.
‡ Nanjing University.
§ E-mail:amiridis@engr.sc.edu.
⊥ E-mail: chenyi@netra.nju.edu.cn.

10.1021/jp046368q CCC: $30.25
Published on Web 01/04/2005

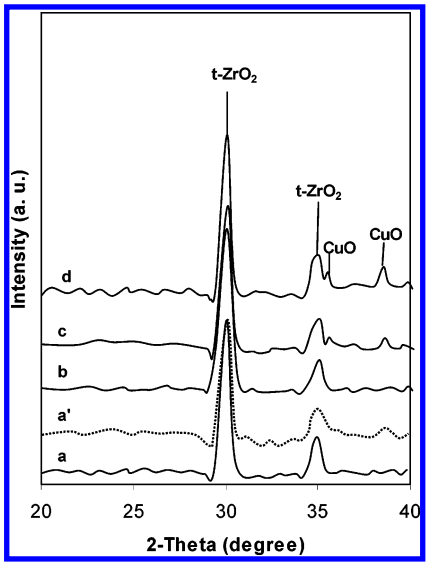

Figure 1. XRD patterns of various CuO/t-ZrO_2 catalysts with different CuO loadings (Cu^{2+} ions/nm^2 t-ZrO_2): (a) 4.9, (b) 7.9, (c) 10.1, (d) 15.3, and (a′) 5 (a physical mixture of CuO and t-ZrO_2).

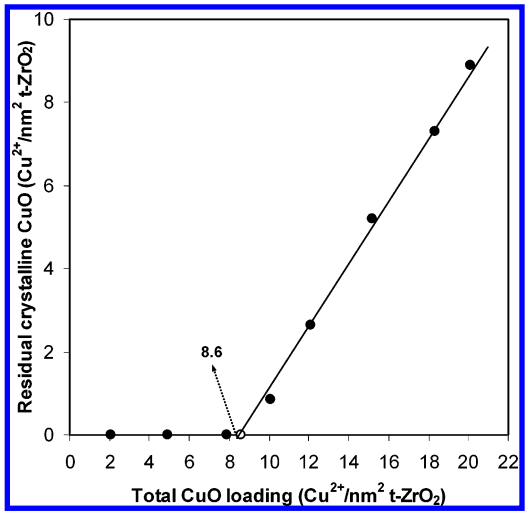

Figure 2. Quantification of the amount of residual crystalline CuO (as determined by XRD patterns) vs CuO loading in various CuO/t-ZrO_2 catalysts.

TABLE 1: Results of XPS Measurements of CuO/t-ZrO_2 Catalysts with Different CuO Loadings

CuO loading (Cu^{2+} nm^{-2} (t-ZrO_2))	binding energy (eV) Cu $2p_{3/2}$	Zr $3d_{5/2}$	XPS intensity ratio ($I_{Cu\ 2p}/I_{Zr\ 3d}$)
1.0	932.6	182.2	0.05
2.1	932.8	182.5	0.11
4.9	932.7	182.3	0.29
7.9	932.8	182.1	0.49
10.1	932.9	182.1	0.55
12.1	933.2	182.2	0.56
15.2	933.5	182.0	0.60
18.3	933.3	182.3	0.64

Kα = 1253.6 eV) was used. The C 1s line (284.6 eV) was used as the reference to calculate the binding energies (BE).

Electron spin resonance (ESR) spectra of precalcined catalysts were recorded with a Bruker ER-200D SRC spectrometer at X-band frequency (9.7667 GHz) and liquid nitrogen temperature.

UV−visible diffuse reflectance (UV/vis−DR) spectra of finely ground samples were recorded in the range of 200−800 nm by a Shimadzu UV-240 spectrophotometer with a $BaSO_4$ sample used as reference.

Temperature-programmed reduction (TPR) measurements were carried out in a quartz U-tube reactor with 40 mg of sample used for each measurement. Prior to the reduction, the sample was pretreated in an air stream at 373 K for 1 h and then cooled to room temperature. Subsequently, a H_2-N_2 mixture (5% H_2 by volume) was introduced to the sample and the temperature was increased linearly at a rate of 10 K min^{-1}. The consumption of H_2 in the reactant stream was monitored by a thermal conductivity detector.

Finally, activity measurements for the catalytic decomposition of N_2O were carried out in a quartz fixed-bed flow reactor using 300 mg of sample. The reactant gas mixture (1% N_2O/He) was introduced at a flow rate of 50 mL/min yielding a space velocity of 10 000 cm^3/g-h. The reaction temperature was maintained at 700 K. The effluent from the reactor was analyzed on line with an SRI 8610 gas chromatograph equipped with a TCD detector and a Carbosphere packed column.

Results and Discussion

Dispersion Capacity and Structure of CuO Supported on t-ZrO_2. The X-ray diffraction patterns of a series of CuO/t-ZrO_2 catalysts with different CuO loadings after calcination at 723 K are shown in Figure 1. The XRD pattern of a physical mixture of CuO and t-ZrO_2 with a 5 Cu^{2+} ions/nm^2 t-ZrO_2 ratio is also presented in this figure for comparison. Two diffraction peaks at $2\theta = 30$ and 34.8°, corresponding to the diffraction of t-ZrO_2,[34] are present in all XRD patterns. The patterns of the low CuO loading samples (i.e., a and b with 4.9 and 7.9 Cu^{2+} ions/nm^2, respectively) do not contain any characteristic peaks that can be assigned to crystalline CuO (i.e., $2\theta = 35.5$ and 38.7 degrees[36]). However, these two XRD peaks can be clearly seen in the patterns of the samples with higher CuO loadings (i.e., 10.1 and 15.3 Cu^{2+} ions/nm^2). The same peaks are also present in the XRD pattern of the physical mixture of CuO and t-ZrO_2, despite the fact that they cannot be observed in the supported catalyst with the same CuO loading. These results indicate that CuO exists in the form of highly dispersed surface species in low CuO loading catalysts, while bulk-type crystalline CuO is formed only in catalysts with higher CuO loadings.

Figure 2 shows the amounts of residual crystalline CuO in CuO/t-ZrO_2 catalysts with different total CuO loadings as determined by quantitative analysis of the corresponding XRD patterns. The presence of XRD-active crystalline CuO becomes evident at samples with a CuO loading at or above 10 Cu^{2+} ions/nm^2 t-ZrO_2. As expected, at relatively higher loadings, the amount of crystalline CuO increases linearly with the CuO loading. Extrapolation of this line to the point of zero residual crystallinity yields the dispersion capacity of CuO on t-ZrO_2 (i.e., approximately 8.6 Cu^{2+} ions/nm^2 t-ZrO_2).

The Cu $2p_{3/2}$ and Zr $3d_{5/2}$ binding energies (as obtained through XPS measurements) of the same series of CuO/t-ZrO_2 catalysts are shown in Table 1. The Zr $3d_{5/2}$ binding energies of all measured catalysts are between182.1 and 182.5 eV, in good agreement with the published data for ZrO_2,[37] and with no systematic deviation observed with CuO loading. In contrast, the Cu $2p_{3/2}$ binding energy appears to correlate with CuO loading, with lower BEs (932.6−932.8 eV) observed for samples containing highly dispersed CuO (i.e., loading below 10 Cu^{2+} ions/nm^2) and higher BEs (933.2−933.5 eV) observed for samples containing crystalline CuO.

Furthermore, it has been reported that metal-to-support intensity ratios obtained by XPS for supported metal oxide

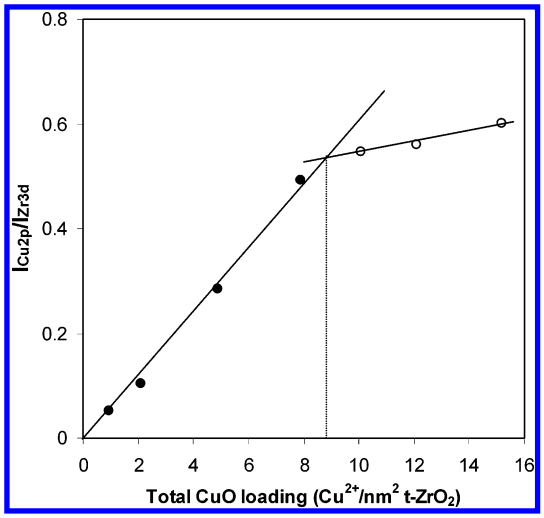

Figure 3. XPS intensity ratios ($I_{Cu\ 2p}/I_{Zr\ 3d}$) as a function of total CuO loading in various CuO/t-ZrO_2 catalysts.

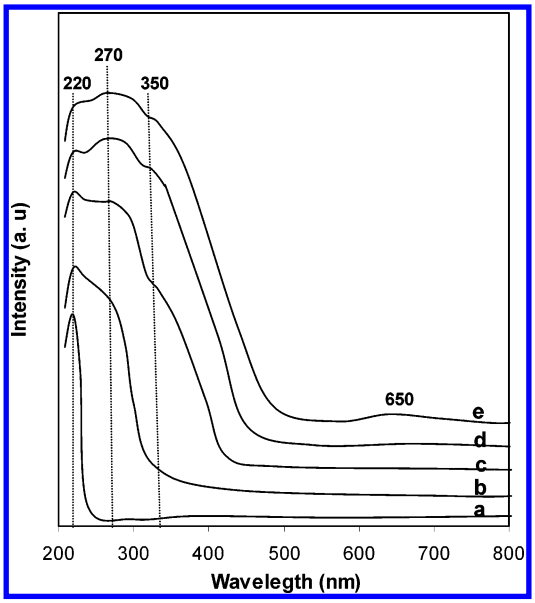

Figure 4. UV/vis−DR spectra of various CuO/t-ZrO_2 catalysts with different CuO loadings (Cu^{2+} ions/nm^2 t-ZrO_2): (a) 0, (b) 2.1, (c) 4.9, (d) 7.9, and (e) 12.1.

samples can provide important information regarding the dispersion and crystallite size of the supported phase.[38,39] Indeed, the Cu 2p/Zr 3d XPS intensity ratios of all catalysts listed in Table 1 correlate linearly with the total CuO loading as shown in Figure 3. In fact, two lines can be drawn for the highly dispersed and crystalline samples with the interception point (at approximately 8.8 Cu^{2+} ions/nm^2 t-ZrO_2), once again corresponding to the dispersion capacity of CuO on t-ZrO_2. This result is in essence identical to the one obtained from the XRD measurements. The apparently different slopes of the two lines in Figure 3 can be rationalized by taking into consideration the differences between the dispersed and crystalline states of CuO on t-ZrO_2. Hence, it is reasonable to expect that for the highly dispersed CuO species the increase in the intensity ratio with CuO loading should be faster than that of the supported bulk-type CuO.

UV/vis−DR spectra of the same series of CuO/t-ZrO_2 catalysts are shown in Figure 4. The spectra of all CuO-containing samples exhibit a strong absorption band at approximately 270 nm with a shoulder at 350 nm. Additionally, the sample with 12.1 Cu^{2+} ions/nm^2 t-ZrO_2 exhibits a weak and

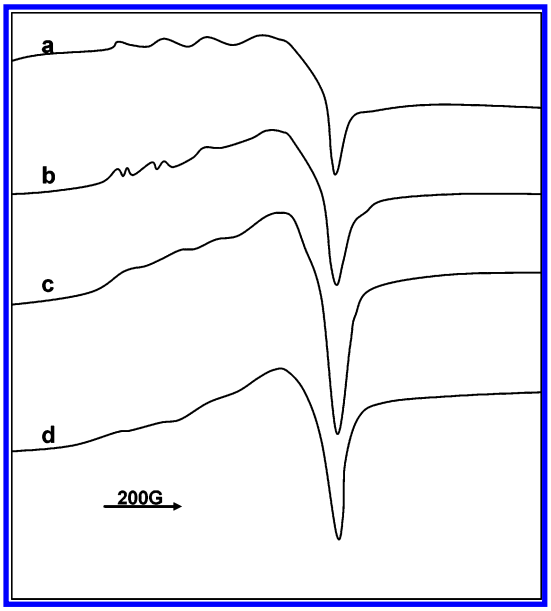

Figure 5. Liquid nitrogen temperature ESR spectra of various CuO/t-ZrO_2 catalysts with different CuO loadings (Cu^{2+} ions/nm^2 t-ZrO_2): (a) 2.1, (b) 4.9, (c) 7.9, and (e) 12.1.

broad band centered at approximately 650 nm. The intensities of the 270 and 350 nm bands increase with CuO loading. According to previous reports,[40,41] the intense band at approximately 270 nm can be assigned to an oxygen to copper charge-transfer, while the 350 nm shoulder can be assigned to highly dispersed Cu^{2+} ion clusters on the zirconia support.[36,42] Finally, the weak and broad band at 650 nm can be assigned to the $^2E_g \rightarrow {}^2T_{2g}$ spin-allowed transition of Cu^{2+} ions in the distorted octahedral sites of cubic crystalline CuO.[42] This band is present only in the sample with a loading above the dispersion capacity of CuO on t-ZrO_2, indicating that CuO crystallites are present only in the high CuO loading samples.[42]

The ESR spectra of the same series of CuO/t-ZrO_2 catalysts after evacuation at room temperature for 1 h are shown in Figure 5. All the spectra can be interpreted in terms of at least two overlapping components. The first one (signal A), with Hamiltonian spin parameters of $g_{\|} = 2.38$, $g_{\perp} = 2.04$, $A_{\|} = 110$ G, and $A_{\perp} = 30-35$ G, has a resolved hyperfine structure visible in the parallel region. Its characteristic line shape can be regarded as an unequivocal proof of the existence of randomly isolated Cu^{2+} ions in an axially symmetric environment.[40,43] The second one (signal B) with $g = 2.23$ consists of a single line shape gradually broadening with increasing CuO loading, and can be assigned to the magnetic interaction of two or more adjacent Cu^{2+} ions. The dipole broadening of these ions probably causes the observed line shape. The above interpretation is consistent with the analysis of Deen et al. for copper oxide supported on alumina.[44]

The observed spectra of the low loading samples are partially resolved in the parallel region, but become poorly resolved with increased CuO loading. Furthermore, at higher CuO loadings, an overlapping and poorly resolved new signal can be seen in the parallel region (as shown in spectrum b of Figure 5), indicating that two kinds of isolated Cu^{2+} ions are located in different symmetric sites of these samples. In addition, when the CuO loading is close to or higher than its dispersion capacity, the signal attributed to the isolated or nearly isolated copper ions in a distorted octahedral environment can hardly be resolved in the parallel region (spectra c and d in Figure 5).

The structure of the dispersed species especially at low CuO loadings is expected to be closely related to the surface structure

of the support. Tetragonal zirconia has a slightly distorted fluorite structure with the (111) plane preferentially exposed on its surface, and each Zr^{4+} ion positioned in a distorted cube of 8-fold oxygen coordination.[45,46] Molecular simulations based on the structural parameters reported by Teufer[47] have revealed the presence of two kinds of surfaces vacant sites (V_I and V_{II}), each coordinated by four oxygen atoms on the (111) plane. As proposed by Chen et al.,[10] the existence of vacant sites on the surface of the support is critical for the dispersion of ionic compounds. Calcination at the appropriate temperature may lead to the incorporation of Cu^{2+} ions into the available vacant sites on the surface, and the accompanying oxygen anions can then "cap" the top of the incorporated Cu^{2+} ions for charge compensation.[18] According to previous reports,[43] copper ions in these two types of available vacant sites have C_{3v} symmetry and can be described as distorted octahedra with a missing corner or as trigonal bipyramids (one elongated and the other compressed).

At very low CuO loadings, the vacant sites (V_I) are more favorable for the incorporation of Cu^{2+} ions since the Cu−O distance (2.045 Å) in this case is very close to that of crystalline CuO (2.09 Å).[43] The presence of only one set of resolved signal in the parallel region of the ESR spectra of the low loading sample in Figure 5a is consistent with such a hypothesis. With the increase of the CuO loading, two sets of $g_{||}$ signals are detected in the ESR spectrum, as shown in Figure 5b. The second signal can be assigned to the contribution of Cu^{2+} ions located in the compressed trigonal bipyramid symmetry discussed in the previous paragraph (however, this signal is poorly resolved in the parallel region and its Hamiltonian spin parameters are rather difficult to calculate). Finally, when the CuO loading reaches the dispersion capacity, all available vacant sites on the support are occupied, hence, almost all previously isolated Cu^{2+} ions are surrounded by additionally incorporated Cu^{2+} ions. As a result, paired Cu^{2+} ions are the predominant surface species. It can be estimated that the distance between the nearest adjacent Cu^{2+} ions in this case is approximately 3.64 Å, a value less than the limit suggested by Centi et al.[40] for generating a dipole interaction between such Cu^{2+} ions. Consequently, the broad ESR line shape of signal B is due to the dipole interaction of such paired ions and can be assigned to these species. Such an assignment is further supported by the fact that the line width and the intensity of this signal do not change with CuO loadings above the dispersion capacity. In short, ESR results indicate that at low CuO loadings, isolated Cu^{2+} ions are the predominant surface species and the ESR signal is relatively well resolved. With increasing CuO loading, paired Cu^{2+} ions become predominant and signal B becomes more broad and intense due to the increasing dipole interactions between adjacent copper ions.

Reducibility of Copper Oxide Species Dispersed on ZrO_2. TPR profiles of CuO/t-ZrO_2 catalysts with CuO loadings ranging between 4.9 and 12.1 Cu^{2+}/nm^2 t-ZrO_2 are shown in Figure 6. The TPR profiles of the catalysts with CuO loadings below the dispersion capacity on t-ZrO_2 (Figure 6, parts a and b) exhibit two reduction peaks at approximately 471 and 477 K. The intensities of these peaks increase with increasing CuO loading up to the dispersion capacity. When the CuO loading exceeds the dispersion capacity, the intensities of these two peaks remain constant, while a new weak peak can be observed at approximately 510 K (Figure 6c). The intensity of this peak gradually increases with CuO loading from 9.6 to 12.1 Cu^{2+}/nm^2 t-ZrO_2, while its position shifts from 510 to 521 K. By comparison with the TPR profile of a physical mixture of CuO and ZrO_2 (Figure 6b′), the peak at 510−521 K can be assigned to the reduction of crystalline CuO, while the peaks at 471 and 477 K can be assigned to the reduction of highly dispersed Cu^{2+} species. The presence of two peaks may indicate a stepwise reduction of the surface-dispersed Cu^{2+} species from Cu^{2+} to Cu^{+} (471 K), closely followed by the reduction from Cu^{+} to Cu^{0} (477 K). A similar behavior has been proposed for the reduction of CuO supported on CeO_2.[48]

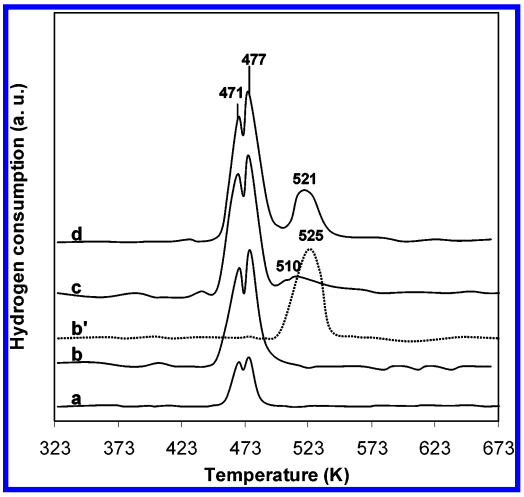

Figure 6. TPR profiles of various CuO/t-ZrO_2 catalysts with different CuO loadings (Cu^{2+} ions/nm^2 t-ZrO_2): (a) 4.9, (b) 7.9, (c) 9.6, (d) 12.1, and (b′) 7.9 (physical mixture of CuO and t-ZrO_2).

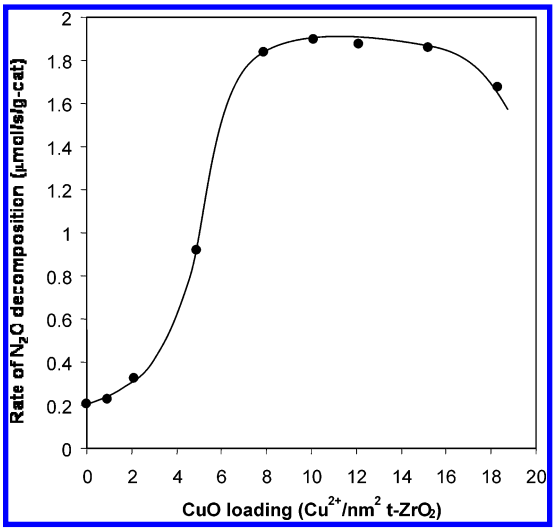

Figure 7. Rate of N_2O decomposition at 700 K over various CuO/t-ZrO2 catalysts as a function of CuO loading.

Reactivity of Copper Oxide Species Dispersed on t-ZrO_2. The catalytic reactivity of CuO supported on t-ZrO_2 was probed through the decomposition of N_2O. The observed N_2O decomposition rate as a function of the CuO loading is shown in Figure 7. For samples with low CuO loadings an increase in the CuO loading has a relatively small effect on the activity, as can be seen from the slope of the corresponding curve in the 0−2.1 Cu^{2+}/nm^2 region. However, the N_2O decomposition rate increases by 1 order of magnitude with an increase of CuO loading from 2.1 to 7.9 Cu^{2+} ions/nm^2 t-ZrO_2 (a value close to the dispersion capacity). Finally, when the CuO loading exceeds the dispersion capacity, no further increase in activity is observed with further increases in the CuO loading.

The catalytic behavior of the CuO/t-ZrO_2 catalysts can be correlated with the previous characterization results. Isolated Cu ions are the predominate surface Cu species on t-ZrO_2 at low CuO loadings. As reported previously, isolated Cu ions on

alumina are poor catalytic sites for the decomposition of N_2O.[49] In fact, it has been proposed that a catalytically active N_2O decomposition site forms when two copper ions occupy neighboring positions on the surface of the support.[49] According to the ESR and UV/vis−DRS results, paired Cu ions appear on the surface of tetragonal zirconia when the CuO loading exceeds a certain value and become the predominant species as the CuO loading approaches the dispersion capacity. These arguments are consistent with the results shown in Figure 7. Furthermore, they can be also used to rationalize the observation that no further significant change in the catalytic activity takes place when the CuO loading exceeds the dispersion capacity of CuO on the t-ZrO_2 support. Eventually, however, the activity decreases for catalysts with CuO loadings higher than 18.3 Cu^{2+} ions/nm^2 t-ZrO_2. Most likely, the increasingly bigger CuO crystallites formed in this case cover some of the active Cu ion sites.

Conclusions

The XRD and XPS results presented in this paper indicate that CuO can be well dispersed on the surface of t-ZrO_2 with a dispersion capacity of approximately 8.6 Cu^{2+} ions/nm^2 t-ZrO_2. Crystalline CuO is formed only when the loading of CuO exceeds the dispersion capacity. ESR and UV/vis-DRS results suggest that two different dispersed copper species are formed on the surface of this support, depending on the CuO loading. At low loadings, isolated copper ions species are predominant, while paired Cu ions become abundant at CuO loadings close to the dispersion capacity. These Cu ion species (both isolated and paired) exhibit a 5-fold-oxygen-coordination symmetry (C_{3v}) and can be described as distorted octahedra with a missing corner or trigonal bipyramids. TPR results reveal that the dispersed Cu ions have a different reducibility from crystalline CuO, presumably due to their interactions with t-ZrO_2. The catalytic activity of the CuO/t-ZrO_2 catalysts for the decomposition of N_2O can be also correlated to dispersion, with the paired Cu ions being the most active sites for this reaction.

References and Notes

(1) Boehm, H. P.; Knozinger, H. In *Analysis, Science and Technology*; Anderson, J. R., Boundart, M., Eds.; Spinger-Verlag: West Berlin, 1983; Vol. 4, p 39.
(2) Yermakov, Yu. I.; Kuznetsov, B. N.; Zakharov, V. A. In *Analysis by Supported Compexes;* Elsevier: Amsterdam, 1981.
(3) Delmon, B.; Houalla, M. *In Preparation of Catalysts II;* Delmon, B., Grange, P., Jacobs, P. A.; Poncelet, G., Eds.; Elsevier: Amsterdam, 1979; p 447.
(4) Xie, Y.; Tang, Y. *Adv. Catal.* **1990**, *37*, 1.
(5) Knozinger, H.; Taglauer, E. In *Catalysis*; Spivey, J. J., Agarqal, S. K., Eds.; A Specialist Periodical Report; The Royal Society of Chemistry: London, 1993; Vol. 10, p1.
(6) Chianelli, R. R.; Daage, M.; Ledouz, M. J. *Adv. Catal.* **1994**, *40*, 177.
(7) Wachs, I. E. *Catal. Today* **1996**, *27*, 437.
(8) Vuurman, M. A.; Wachs, I. E. *J. Phys. Chem.* **1992**, *96*, 5008.
(9) Liu, Z.; Chen, Y. *J. Catal.* **1998**, *177*, 314.
(10) Chen, Y.; Dong, L.; Jin, Y.; Xu, B.; Ji, W. In *Studies in Surface Science Catalysis*; Hightower, J. W., Delgass, W. N., Iglessia, E.; Bell, A. T., Eds.; Elsevier Science: New York, 1996; Vol. 101, p 1293.
(11) Kim, T.-W.; Song, M.-W.; Koh, H.-L.; Kim, K.-L. *Appl. Catal., A* **2001**, *210*, 35.
(12) Weigel, J.; Frohlich, C.; Baiker, A.; Wokaun, A. *Appl. Catal., A* **1996**, *140*, 29.
(13) Velu, S.; Suzuki, K.; Okazaki, M.; Kapoor, M. P.; Osaki, T.; Ohashi, F. *J. Catal.* **2000**, *194*, 373.
(14) Martinez-Arias, A.; Ferandez-Garcia, M.; Galvez, O.; Coronado, J. M.; Anderson, J. A.; Consea, J. C.; Soria, J.; Munnera, G. *J. Catal.* **2000**, *195*, 207.
(15) Brands, D. S.; Poels, E. K.; Bliek, A. *Appl. Catal., A* **1999**, *184*, 279.
(16) Tavares Figuerirdo, R.; Martinez-Arias, A.; Lopez Granados, M.; Fierro, J. L. G. *J. Catal.* **1998**, *178*, 146.
(17) Fabina, M. T.; Schmal, M. *Appl. Catal., A* **1997**, *163*, 153.
(18) Fridman, V. Z.; Davydov, A. A. *J. Catal.* **2000**, *195*, 20.
(19) Sohn, J. R.; Cho, S. G.; Pae, Y.; Hayashi, S. *J. Catal.* **1996**, *159*, 170.
(20) Chen, K.; Fan, Y.; Hu, Z.; Yan, Q. *Catal. Lett.* **1996**, *36*, 139.
(21) Kim, D. S.; Wachs, I. E. *J. Catal.* **1993**, *142*, 166.
(22) Liu, H. C.; Cheung, P.; Iglesia, E. *J. Phys. Chem., B* **2003**, *107*, 4118.
(23) Chen, K. D.; Bell, A. T.; Iglesia, E. *J. Catal.* **2002**, *209*, 35.
(24) Fisher, I. A.; Woo, H. C.; Bell, A. T. *Catal. Lett.* **1997**, *44*, 11.
(25) Koeppel, R. A.; Baiker, A.; Wokaum, A. *Appl. Catal., A* **1992**, *84*, 77.
(26) Sun, Y.; Sermon, P. A. *Catal. Lett.* **1994**, *29*, 361.
(27) Centi, G.; Perathoner, S. *Appl. Catal., A* **1995**, *132*, 179.
(28) Lin, J.; Chen, H. Y.; Chen, L.; Tan, K. L.; Zeng, H. C. Appl. *Surf. Sci.* **1996**, *103*, 307.
(29) Miller, T. M.; Grassian, V. H. *Colloids Surf., A* **1995**, *105*, 113.
(30) Kramlich, J. C.; Linak, W. P. Prog. *Energy Combust. Sci.* **1994**, *20*, 149.
(31) Wojtowicz, M. A.; Pels, J. R.; Moulijn, J. A. *Fuel Proc. Technol.* **1993**, *34*, 1.
(32) Centi, G.; Cerrato, G.; D'Angelo, S.; Finardi, U.; Giamello, E.; Morterra, C.; Perathoner, S. *Catal. Today* **1996**, *27*, 265.
(33) Morterra, C.; Giamello, E.; Cerrato, G.; Centi, G.; Perathoner, S. *J. Catal.* **1998**, *179*, 111.
(34) Liu, Z.; Ji, W.; Dong, L.; Chen, Y. *J. Solid State Chem.* **1998**, *138*, 41.
(35) Liu, Z.; Ji, W.; Dong, L.; Chen, Y. *Mater. Chem. Phys.* **1998**, *56*, 134.
(36) Dong, L.; Hu, Y.; Shen, M.; Jin, T.; Wang, J.; Ding, W.; Chen, Y. *Chem. Mater.* **2001**, *13*, 4227.
(37) Sarma, D. D.; Rao, C. N. R. *J. Electron Spectrosc. Relat. Phen.* **1980**, *20*, 25.
(38) Kerkhof, F. P. J. M.; Moulijn, J. M. *J. Phys. Chem.* **1979**, *83*, 1612.
(39) Fung, S. C. *J. Catal.* **1979**, *58*, 454.
(40) Centi, G.; Perathoner, S.; Biglino, D.; Giamello, E. *J. Catal.* **1995**, *151*. 75.
(41) Marion, M. C.; Garboeski, R.; Primet, M. *J. Chem. Soc., Faraday Trans.* **1990**, *86*, 3027.
(42) Chary, K. V. R.; Seela, K. K.; Sega, G. V.; Sreedhar, B. *J. Phys. Chem., B* **2004**, *108*, 658.
(43) Liu, Z.; Ji, W.; Dong, L.; Chen, Y. *J. Catal.* **1997**, *172*, 243.
(44) Deen, R.; Scheltus, P. T.; Vries, G. *J. Catal.* **1976**, *41*, 412.
(45) Anderson, J. R. *Structure of Metallic Catalysts*; Academic Press: London/New York/San Francisco, 1975, p 62.
(46) Morterra, C.; Cerrato, G.; Ferroni, L.; Montanaro, L. *Mater. Chem. Phys.* **1994**, *37*, 243.
(47) Teufer, G. *Acta Crystallogr.* **1962**, *15*, 1187.
(48) Dong, L.; Jin, S. Y.; Chen, Y. *Sci. China, Ser. B* **1997**, *40*, 24.
(49) Zhu, Z. H.; Zhu, H. Y.; Wang, S. B.; Lu, G. Q. *Catal. Lett.* **2003**, *91*, 73.